The Influence of Shoal/Channel Interactions in a Shallow, Macrotidal Estuary on Frontogenesis, Transverse Circulations, and Vertical Mixing

Sarah N. Giddings[1], Derek A. Fong[2], Stephen G. Monismith[3], Kathleen A. Edwards[4], and Andrew T. Jessup[5]

Introduction

The dynamics of the Snohomish River Estuary, Everett, WA are examined utilizing in-situ and remote sensing data collected during July 2006. Results from the field experiment highlight the need for understanding shoal/channel interactions in order to interpret tidally averaged quantities. Four moorings (M2A, M2B, M3A, and M3B) with bottom mounted acoustic Doppler current profilers (ADCP); acoustic Doppler velocimeters (ADV); and conductivity, temperature, depth (CTD) sensors at three depths were deployed for over twenty days along with two additional moorings (M4 and M6) with a bottom mounted ADCP and CTD. The moorings along with high resolution ADCP and CTD transecting surveys and an autonomous underwater vehicle, REMUS, are utilized to examine the interactions between complex bathymetry induced frontogenesis, transverse circulations, and vertical mixing and stratification. Concurrent infrared remote sensing from both near-field oblique views as well as far-field aerial imagery supplements the in-situ instrumentation and helps corroborate the frontogenesis mechanism.

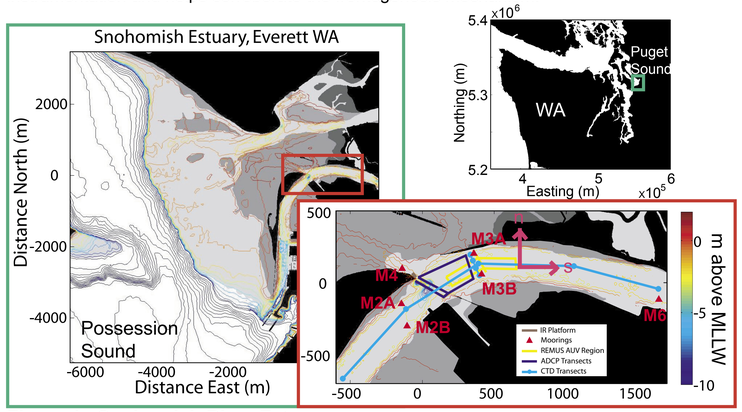

Figure 1. Snohomish River Estuary, Everett, WA map and mooring locations

Snohomish River Estuary

The Snohomish River Estuary is characterized by strong tidal currents exceeding 1.5m/s, complex bathymetry including extensive intertidal mudflats and shallow channels (1.5-2m deep at lower low water), a large tidal range (>4m during spring tides) and a sharp salt-wedge. The Snohomish River flow varies seasonally with daily medians ranging from 60 to 300 m^3/s (USGS 2007). Water level is dominated by the M_2 semidiurnal and K_1 diurnal tidal constituents. The tides are near standing waves with a slightly progressive nature (slack water occurs ~20 min after high tide.) The tidal influence is felt beyond 30km upstream (USGS 2007), while the maximum salt-wedge intrusion is about 12km upstream (Fram et al. 2003).

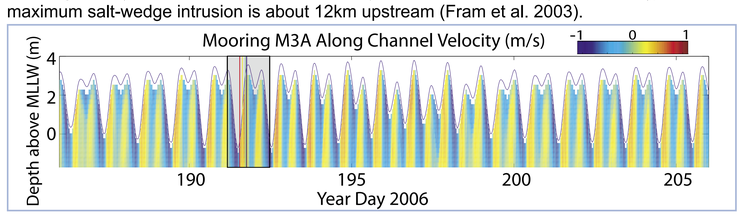

Figure 2. Along Channel Velocity (m/s) recorded by bottom mounted ADCP at Mooring M3A. Thirty-hour spring survey is highlighted in gray.

Frontogenesis and Propagation

A reoccurring surface convergence front forms off the northern tip of Jetty Island where the mudflats meet the main channel during flood tides. The front is accompanied by a visible foam/debris convergence line. The front appears around mid flood tide after lower low water as a convergence front separating the flooding mudflat water from the flooding main channel. The front propagates across the channel, eventually passing over mooring M3B just before it dissipates at high water. The front has a clear thermal structure evident in infrared images.

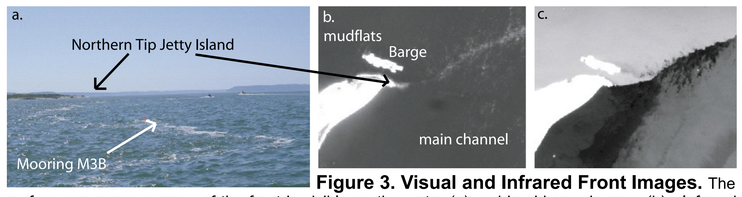

Figure 3. Visual and Infrared Front Images. The surface convergence zone of the front is visible on the water (a) and in airborne images (b). Infrared imagery (c) shows convergence of water masses with different thermal signatures. Water flooding from the mudflats is warmer (lighter gray), than that from the main channel. Photograph a is looking towards the mudflats and the airborne images are rotated with North up. Images were taken during peak flood.

Transverse Circulations

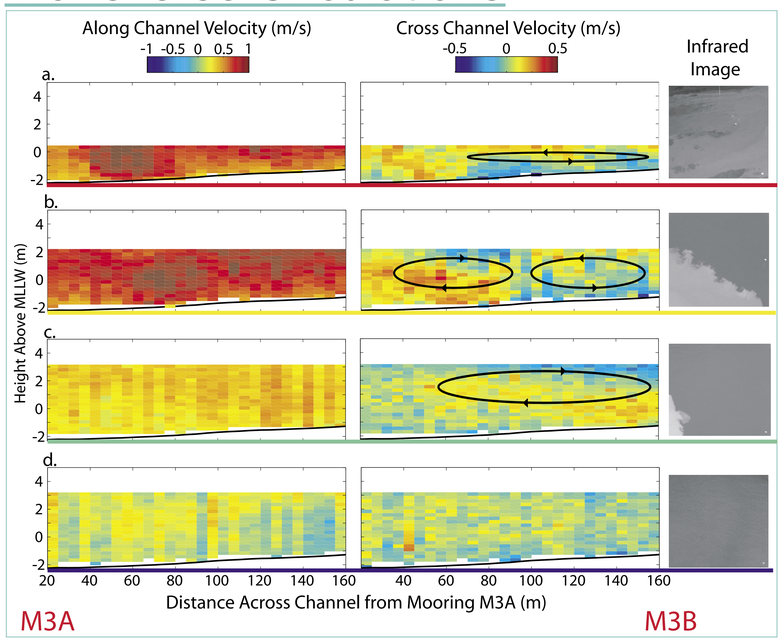

Figure 4. Transverse Circulations during the Frontal Development and Breakdown. ADCP transects between Moorings M3A and M3B during the spring thirty-hour survey flood tide before (a), during (b, c), and after (d) the frontal presence. Currents are rotated into along (left panel) and across (middle panel) channel directions using principle axes analysis. Flood tide and currents towards the outer bank are positive as sketched in figure 1. Transects face upstream with mooring M3A on the left and M3B on the right. The Infrared Images (not georectified) to the right are taken within 1 minute of the transect. This series of data shows the development and competition of two surface-convergent circulation cells corresponding with the front.

Both the fixed velocity measurements at moorings M3A, M3B, and M4 as well as ADCP transects between Moorings M3A and M3B elucidate the transverse circulations associated with this convergence front. Prior to frontogenesis, secondary circulation is directed in the sense expected due to channel curvature. During the flood tide, a second circulation cell develops in the opposite sense. These circulation cells form a convergent front at the surface. As the surface convergence front propagates across the channel, so does the outer bank circulation cell eventually creating circulation across the channel that is opposite that expected by curvature. This is followed by a decrease in the currents and breakdown of both the secondary circulation and the front.

The lateral momentum equation in curvilinear coordinates is:

$$\frac{\partial u_n}{\partial t} + u_s\frac{\partial u_n}{\partial s} - \frac{u_s^2}{R_s} + fu_s + g\frac{\partial \eta}{\partial n} + \frac{g}{\rho_o}\left(\frac{\partial}{\partial n}\int_z^0 \rho(z')dz'\right) - \frac{\partial}{\partial z}\left(A_z\frac{\partial u_n}{\partial z}\right) = 0$$

acceleration | advection | centrifugal (curvature) | Coriolis (rotation) | barotropic | baroclinic | friction

Scaling the lateral momentum equation, the dominant terms in this system are the centrifugal, baroclinic, and friction terms (barotropic term could not be estimated at this time). A more in depth look at each term over the course of the tidal cycle (not shown here) shows that the baroclinic forcing term becomes increasingly important over the development and breakdown of the front, first balancing the centrifugal forcing, and then overtaking it.

Examining the moored CTD arrays, transverse CTD transects, and transverse autonomous underwater vehicle transects, the density difference across the front is strong with less dense water and more stratification on the outer bank as corroborated by the infrared images. This difference in density and stratification is what leads to the baroclinic pressure gradient.

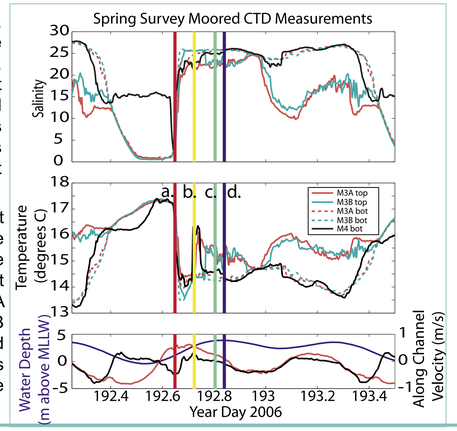

Figure 5. Mudflat Trapping. CTDs at moorings M3A, M3B and M4 show the trapping effect of the mudflats and the pulse of mid-density water first at M3A and then at M3B after the relaxation of the front. M3A is stratified when the front is present. M3B becomes stratified after the front has passed over it. Moored velocity measurements show flow reversal and a subsequent pulse towards the main channel in the mudflats.

Vertical Mixing and Stratification

During the presence of the front, the outer bank is stratified enough to withstand vertical mixing while the inner bank is able to mix throughout the water column. When the front breaks down, the entire channel becomes stratified and that in addition to decreased currents suppresses mixing across the channel. The differential stratification between the outer and inner banks directly creates a baroclinic force opposing curvature and it can interact with the centrifugal forcing indirectly to further enhance the baroclinic forcing. Additionally, the differential mixing can further enhance the front.

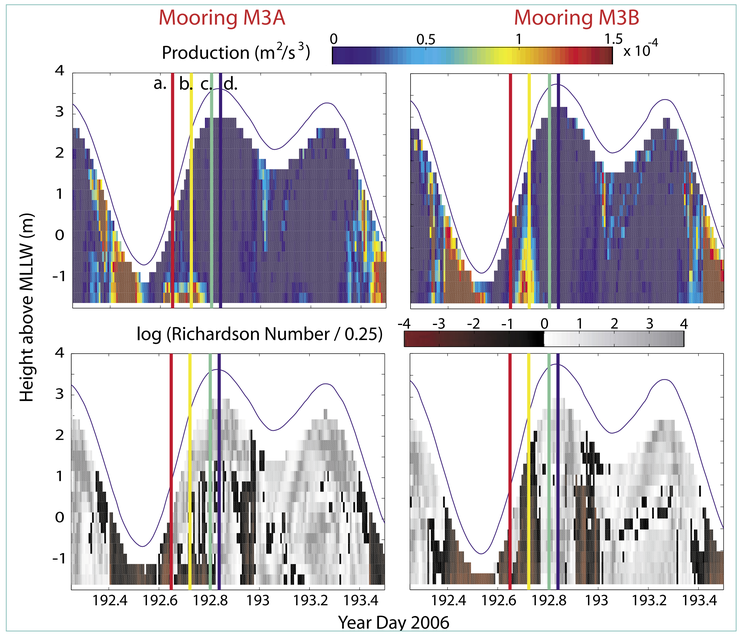

Figure 6. Turbulent Kinetic Energy Production and Richardson Number. Turbulent Kinetic Energy Production is computed with ADCP variance method Reynolds stresses. Richardson Number is computed with moored CTD derived buoyancy and shear from the ADCPs. log(Ri/0.25) indicates anything greater than zero is considered stable, while anything less than zero is subject to mixing. Note that while the front is present, the inner bank (Mooring M3A) cannot mix throughout the water column while the outer bank is susceptible to shear.

Summary

Synthesizing our moored, transecting, and autonomous measurements, we can form a complete picture of frontogenesis and how this front influences vertical stratification and mixing in the Snohomish. During ebb tides, the mudflats are cut off from Possession Sound trapping mid-density water. During flood tide after lower low water, when the mudflats reconnect to Possession Sound, the mid density mudflat water converges with the main channel flooding dense Possession Sound water. This pulse of intermediate density water induces a baroclinic forcing which competes with the centrifugal forcing to form two strong convergent circulation cells. While the front is present, the outer bank is more stratified than the inner bank and therefore is less susceptible to mixing. When the along channel currents decrease, the centrifugal acceleration becomes small (as does bottom generated turbulence and shear) and the lighter water on the outer bank quickly moves across the channel. This mechanism is similar to that found by Lacy et al. 2003 and reemphasizes the complex interactions between secondary circulations, vertical mixing, and stratification. This front acts as a mixing mechanism incorporating trapped mid-density water into the system. This shoal/channel interaction has direct implications for circulation and mixing in the Snohomish and suggests the importance of shoal/channel interactions in other systems.

References

Fram, J. P., G. P. Gerbi, W. R. Geyer and P. MacCready, 2003: Longitudinal and lateral salt gradients of the Snohomish river estuary: Summer research project at Friday Harbor laboratories.

Lacy, J. R., M. T. Stacey, J. R. Burau, and S. G. Monismith, 2003: Interaction of lateral baroclinic forcing and turbulence in an estuary. Journal of Geophysical Research, 108 (C3), 3089-3103.

United States Geological Survey, 2007: USGS real-time water data. http://waterdata.usgs.gov/nwis/rt

Acknowledgements

Thanks to ONR and NSF for support and the generous help of the Stanford Environmental Fluid Mechanics Laboratory students for many long hours in the field.

Contact Information

1 Civil & Environmental Engineering, Stanford University, sarahgid@stanford.edu
2 Civil & Environmental Engineering, Stanford University, dfong@stanford.edu
3 Civil & Environmental Engineering, Stanford University, monismith@stanford.edu
4 Applied Physics Laboratory, University of Washington, edwards@apl.washington.edu
5 Applied Physics Laboratory, University of Washington, jessup@apl.washington.edu